Catalysis Today 149 (2010) 143–147

Contents lists available at ScienceDirect

Catalysis Today

journal homepage: www.elsevier.com/locate/cattod

High effective dehydration of bio-ethanol into ethylene over nanoscale HZSM-5 zeolite catalysts

Jiandong Bi, Xinwen Guo *, Min Liu, Xiangsheng Wang

State Key Lab of Fine Chemicals, Department of Catalysis Chemistry and Engineering, School of Chemical Engineering, Dalian University of Technology, P.O. Box 39, No. 158 Zhongshan Road, Dalian, Liaoning 116012, China

ARTICLE INFO

Article history:
Available online 2 June 2009

Keywords:
Dehydration
Bio-ethanol
Ethylene
Nanoscale HZSM-5
Stability

ABSTRACT

Nanoscale and microscale HZSM-5 zeolite catalysts were prepared and characterized by using SEM, XRD, IR, TPD and modified Hammett indicator method. Their performances in the dehydration of bio-ethanol into ethylene were compared in a fixed-bed reactor at 240 °C under atmospheric pressure. The results show that nanoscale HZSM-5 zeolite catalyst exhibits better stability than microscale HZSM-5 zeolite catalyst. When the 95(v) % bio-ethanol is used as the reactant, over nanoscale HZSM-5 catalyst, the conversion of bio-ethanol and the selectivity for ethylene almost keep constant during 630 h reaction, while over microscale HZSM-5 zeolite catalyst, the conversion of bio-ethanol decreases after 60 h reaction; in the case of the 45(v) % bio-ethanol employed as the feedstock, over nanoscale HZSM-5 catalyst, the conversion of bio-ethanol and the selectivity for ethylene almost keep constant during 320 h reaction, while over microscale HZSM-5 zeolite catalyst, both the conversion of bio-ethanol and the selectivity for ethylene decrease almost at the beginning of the reaction.

1. Introduction

Owing to energy crisis and effect of greenhouse, more and more researchers have paid more attention to the conversion of biomass in recent years, for example, the production of bio-ethanol (from biomass fermentation), the production of bio-diesel, the conversion of glycerol and the dehydration of bio-ethanol into ethylene, etc. It has been well known that the dehydration of ethanol into ethylene could be catalyzed by HZSM-5 zeolite catalysts, and the temperature of this reaction over HZSM-5 zeolite catalysts was lower than that over alumina catalysts, however, the application of alumina catalysts for this reaction is still dominant industrial process, despite its high energy-cost and low productivity (375–450 °C, 0.13 h^{-1}) [1]. The possible reason is that the stability of microscale HZSM-5 zeolite catalyst is not satisfactory. So, developing catalysts with high efficiency under lower reaction temperature to substitute alumina catalyst is desirable.

There are many reports on the selective production of ethylene from ethanol over microscale HZSM-5 zeolite catalyst. Le Van Mao and co-workers reported the biomass-ethanol-to-ethylene (BETE) process based on HZSM-5 zeolite catalysts modified with trifluoromethanesulfonic acid (TFA), Zn–Mn, La/Ce cations, and asbestos, respectively [2–7]. Pan et al. revealed that microscale HZSM-5 zeolite catalyst exhibited good catalytic stability only when the reaction temperature is above 300 °C. In order to keep the catalytic stability, the reaction temperature needs to be increased continuously [8]. Moser et al. investigated the catalytic performance of HZSM-5 zeolite catalysts with the ratio of Si/Al from 30 to 15,000 at the temperature scope from 200 °C to 500 °C using 20–95(v) % ethanol solutions as the reactant [9]. Sawane Bun et al. studied the catalytic performance of the ion-exchanged HZSM-5 zeolite catalyst at temperature ranging from 227–527 °C [10]. Phillips et al. reported the production of ethylene from ethanol solution on HZSM-5 zeolite catalyst under mild conditions [11]. Recently, Zhang et al. demonstrated the effect of P content on the conversion of ethanol over HZSM-5 zeolite catalyst [12]. However, there are no reports on the stability of HZSM-5 zeolite catalyst in the dehydration of ethanol into ethylene when the reaction temperature is below 300 °C. Nanoscale HZSM-5 zeolite is a good acid-catalyst, which exhibits good coke-resistance and stability in many other reactions [13–16]. Therefore, in this paper, the dehydration of bio-ethanol into ethylene was investigated over nanoscale HZSM-5 zeolite catalyst in a fixed-bed reactor at 240 °C under atmospheric pressure.

2. Experimental

2.1. Catalyst preparation

Nanoscale HZSM-5 zeolite powder (crystal size: 50–100 nm; SiO_2/Al_2O_3 = 26) was prepared according to the previous literature

* Corresponding author. Tel.: +86 411 88993990; fax: +86 411 83633080.
E-mail address: guoxw@dlut.edu.cn (X. Guo).

0920-5861/$ – see front matter © 2009 Elsevier B.V. All rights reserved.
doi:10.1016/j.cattod.2009.04.016

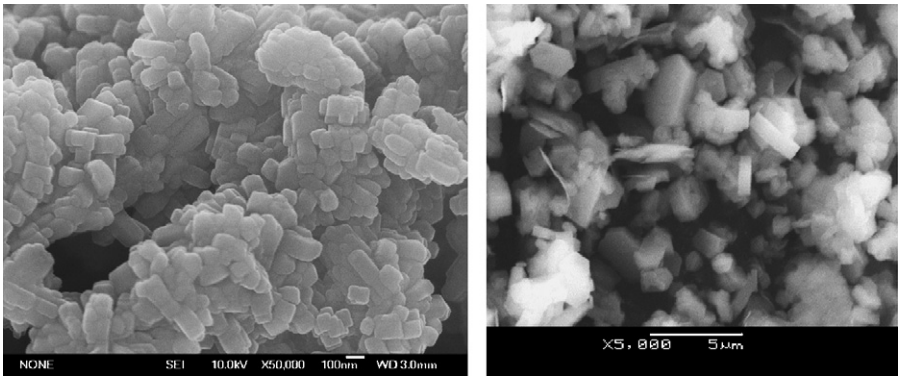

Fig. 1. SEM photographs of nanoscale HZSM-5 zeolite (left) and microscale HZSM-5 zeolite (right).

[17]. By using a 0.5 mol/L HNO_3 solution as adhesive and extruding the mixture of 70 wt% nanoscale HZSM-5 (powder) with 30 wt% alumina (powder), the strip of nanoscale HZSM-5 catalyst was formed. After dried at room temperature for 15 h and calcined at 540 °C for 4 h, the nanoscale HZSM-5 zeolite catalyst labeled as nano-CAT was obtained. In order to make a comparison, the corresponding microscale HZSM-5 zeolite catalyst labeled as micro-CAT was also prepared. The microscale HZSM-5 zeolite powder (crystal size: 1–3 μ; $SiO2/Al_2O_3$ = 25) was commercially available (Nankai University, China). All of the catalyst strips were crushed to 20–30 mesh before catalytic test.

2.2. Catalyst characterization

The crystal size and morphology of the nanoscale HZSM-5 and microscale HZSM-5 were obtained on a JEOL JSM-6700 F scanning electron microscope. The XRD patterns were recorded on a D/max-2400 diffractometer with a scanning rate of 4°/min from 5° to 50°. The acid properties of the catalyst samples were obtained on a Quantachrome CHEMBET 3000 using the NH_3-TPD method. IR spectra were recorded on an EQUINOX55 Fourier transform infrared spectrometer (Bruker Corp.) at 4 cm^{-1} resolution. The samples were finely ground and pressed into a self-supporting wafer (8–10 mg/cm^2, diameter 10 mm). For Py-IR spectra, after evacuation under vacuum for 2 h, a background spectrum was measured and then the samples were exposed to pyridine at room temperature for 10 min. The wafers containing pyridine were desorbed under vacuum at 250 °C, and then the IR spectra were measured again. The acid strength distribution of the catalyst samples was measured by modified Hammett indicator method using methyl red (pKa = +4.8) and p-aminoazobenzene (pKa = +2.27) as indicators. The titration procedure with n-butylamine and cyclohexylamine was described in details in the previous literature [18]. The coke content in the used catalysts was determined by combustion in a thermogravimetric (TG) analyzer. The temperature was raised from 40 °C to 850 °C with a ramp of 10 °C/min.

2.3. Catalytic test

The dehydration was carried out in a vertical, down-flow, fixed-bed reactor (length 40 cm and inner diameter 0.8 cm) under atmospheric pressure. The 95(v) % bio-ethanol (commercially available) was used as received, and the 45(v) % bio-ethanol was from the 95(v) % bio-ethanol diluted with distilled water. Catalyst (1 g) was loaded in the identical temperature zone (the middle of the reactor), and the inert porcelain clay was packed in the rest of reactor. The temperature of the catalyst, controlled with a thermocouple at the position of the identical temperature zone, was raised to the given temperature in a flow of N_2 gas. Catalyst was activated at 450 °C for 2 h before reaction. After the catalyst activation, the 95(v) % bio-ethanol (liquid) was fed into the reactor along with N_2 gas (35 ml/min). When the 45(v) % bio-ethanol was employed as the reactant, carrier-gas was stopped. The WHSV based on the component of ethanol was 1 h^{-1} for the 95(v) % feedstock, and that was 0.8 h^{-1} for the 45(v) % feedstock.

The gas effluent was analyzed by FID gas chromatograph (equipped with a 4 mm × 2 m GDX103 packed column) which was directly connected to the top of a gas–liquid separator, and the trapped liquid was analyzed by TCD gas chromatograph (equipped with a 2 mm × 3 m GDX101 packed column). The components of gas effluent were ethylene, methane, ethane, acetaldehyde, unreacted ethanol, diethyl ether, higher aliphatic hydrocarbon (C_3–C_8) and aromatics; the components of the trapped liquid were water, unreacted ethanol and very small amount of acetaldehyde or diethyl ether.

The conversion of ethanol was defined as [molar amount of converted ethanol]/[molar amount of ethanol in the feedstock]. The selectivity of ethylene was defined as [molar amount of ethanol converted to ethylene]/[molar amount of converted ethanol].

3. Results and discussion

3.1. Characterization of catalyst

Fig. 1 is the SEM photographs of nanoscale and microscale HZSM-5 zeolites. It is shown that the crystal size of nanoscale HZSM-5 is in the range of 50–100 nm and that of microscale HZSM-5 is in the range of 1–3 μm. The XRD patterns of catalyst samples are shown in Fig. 2. It is confirmed that both of the samples are

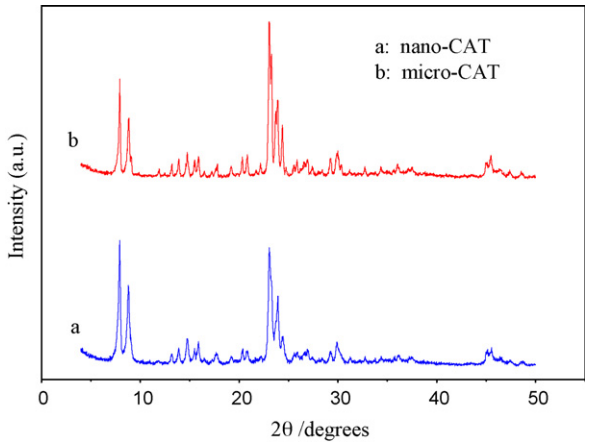

Fig. 2. XRD patterns of nano-CAT and micro-CAT.

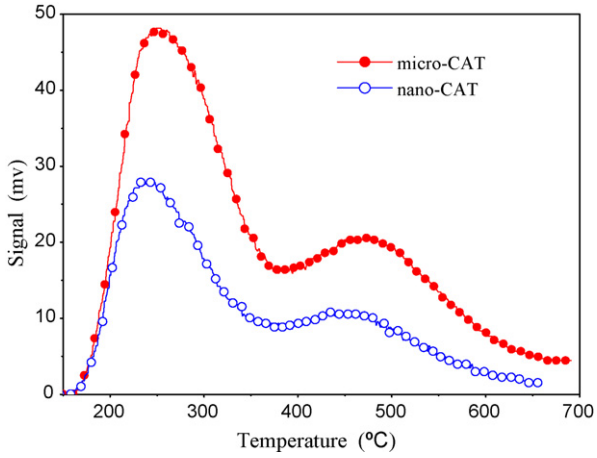

Fig. 3. TPD curves of nano-CAT and micro-CAT.

typical MFI-type structure. NH_3-TPD curves of catalyst samples are given in Fig. 3. Generally, there are two NH_3-desorption peaks for HZSM-5 zeolite. The peak at higher temperature is attributed to the desorption of ammonia chemisorbed at strong acid sites, and that at lower temperature is assigned to weak acid sites. Form Fig. 3, it is apparent that the acid sites in the micro-CAT are more than that in the nano-CAT. Fig. 4 is the FT-IR spectra of pyridine desorption at 250 °C over the catalyst samples. The peaks of 1545 cm^{-1} and 1455 cm^{-1} correspond to the bonds of Brønsted–pyridinium ion and pyridine coordinated to Lewis sites, respectively [19]. The percentage of Brønsted acid sites in the total number of acid sites (Brønsted acid sites + Lewis acid sites) on each of the tested samples was estimated from the integrated peak areas of the two absorption bands of the catalyst [20]. The percentage of Brønsted acid sites on nano-CAT was estimated to be 63%, and that of micro-CAT was 68%. The acid strength distributions of the catalyst samples by Hammett Indicator method are given in Table 1. As shown in Table 1, the amount of the acid sites ($H_0 \leq +4.8$) on the external surface of nano-CAT is more than that of micro-CAT. It can be deduced that the ratio of the strong acid sites inside the zeolite channels to the total strong acid sites ($H_0 \leq +2.27$) is 50% for the nano-CAT, and that is 90% for the micro-CAT. This indicates that for the micro-CAT, most of the strong acid sites locate in the zeolite channels, and only small part of them locates on the outer surface of zeolite, while for the nano-CAT, about half of the strong acid sites locates on the outer surface of zeolite.

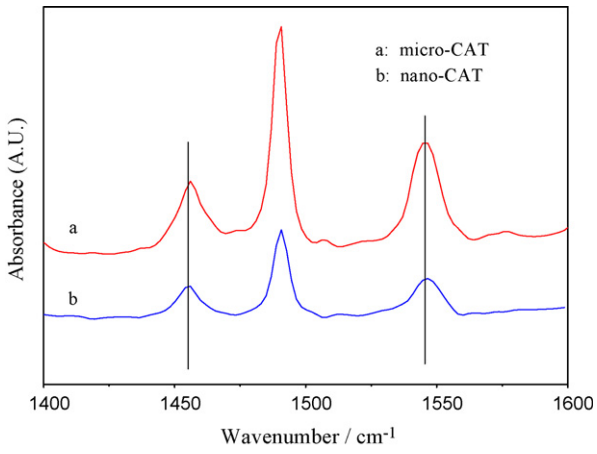

Fig. 4. FT-IR spectra of pyridine desorption at 250 °C over the catalyst samples.

Table 1
Acid strength distributions of the catalyst samples.

Catalyst	Acid sites[a] on the external[b] surface mmol/g		Total acid sites mmol/g		External/ total %	
	$H_0 \leq +2.27$	$H_0 \leq +4.8$	$H_0 \leq +2.27$	$H_0 \leq +4.8$	$H_0 \leq +2.27$	$H_0 \leq +4.8$
Nano-CAT	0.05	0.30	0.10	0.80	50	37.5
Micro-CAT	0.01	0.10	0.10	1.30	10	8

[a] The acid site was measured by the modified Hammett indicator.
[b] Including the acid sites in the pore mouth of HZSM-5.

3.2. Catalytic performance in dehydration of bio-ethanol

The catalytic performances of nanoscale HZSM-5 and micro-scale HZSM-5 catalysts in the dehydration of bio-ethanol were investigated using different concentration of bio-ethanol in the fixed-bed reactor and the results are given in Figs. 5 and 6. Figs. 5 and 6 show the relationship of the catalytic performance vs. time on stream over nano-CAT and micro-CAT catalysts in the dehydration of 95(v) % bio-ethanol, respectively. Over nano-CAT catalyst, the conversion of bio-ethanol and the selectivity for ethylene almost keep constant during 630 h reaction; the conversion of bio-ethanol gradually decreases from 99.20% to 98.40%, and the selectivity for ethylene decreases from 98.69% to

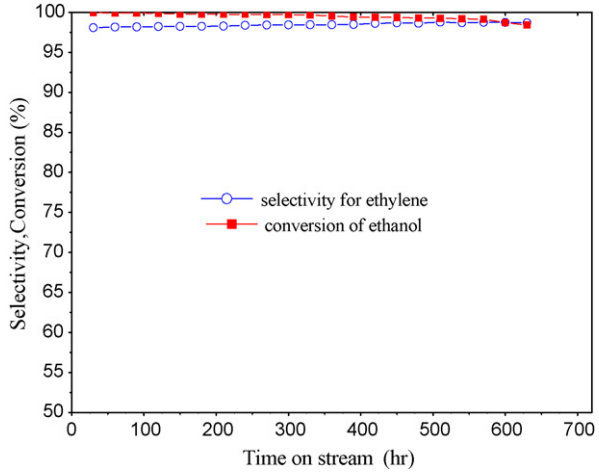

Fig. 5. Catalytic performance for the nano-CAT/95(v) % bio-ethanol, temperature/ 240 °C.

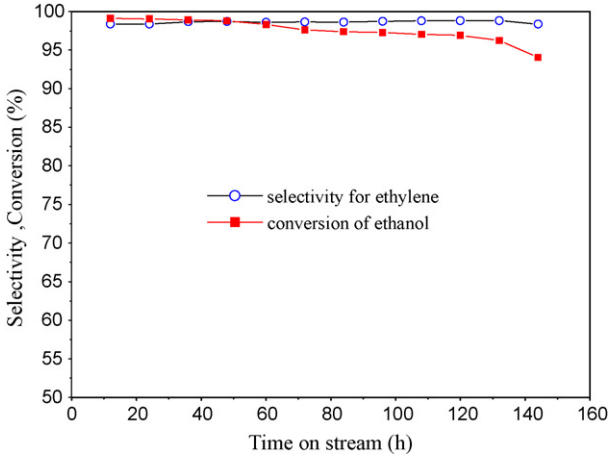

Fig. 6. Catalytic performance for the micro-CAT/95(v) % bio-ethanol, temperature/ 240 °C.

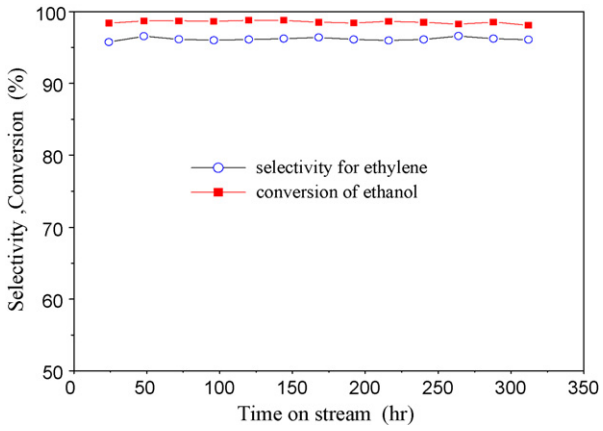

Fig. 7. Catalytic performance for the nano-CAT/45(v) % bio-ethanol, temperature/240 °C.

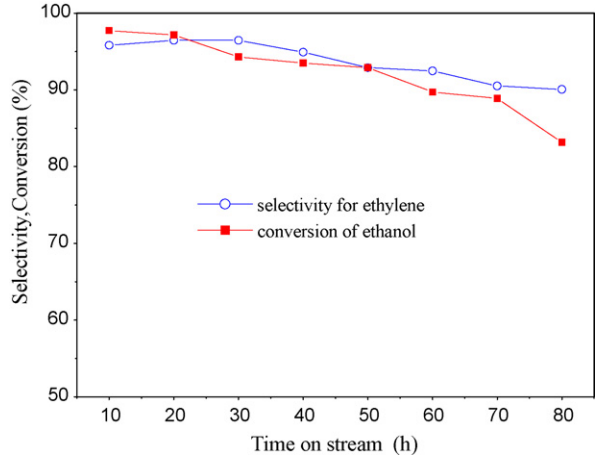

Fig. 8. Catalytic performance for the micro-CAT/45(v) % bio-ethanol, temperature/240 °C.

98.43% when the time on stream increases from 420 h to 630 h. Over micro-CAT catalyst, the conversion of bio-ethanol decreases after 60 h reaction.

Figs. 7 and 8 show the relationship of the catalytic performance vs. time on stream over nano-CAT and micro-CAT catalysts for the dehydration of 45(v) % bio-ethanol, respectively. Over nano-CAT catalyst, the conversion of bio-ethanol and the selectivity for ethylene almost keep constant during 320 h reaction; while over micro-CAT catalyst, both the conversion of ethanol and the selectivity for ethylene decrease almost at the beginning of the reaction.

Product distributions over nanoscale HZSM-5 and microscale HZSM-5 catalysts were given in Table 2. In the dehydration of bio-ethanol, the product distribution over nanoscale HZSM-5 catalyst is similar to that over microscale HZSM-5 catalyst. In the gas phase products, ethylene is the main product. Small amount of byproducts, such as diethyl ether from the intermolecular dehydration of bio-ethanol and hydrocarbons from cracking or polymerization, was also detected. From Table 2, it can be further demonstrated that nanoscale HZSM-5 catalyst exhibits high stability.

3.3. Discussion

The stability is associated with the catalyst deactivation. It is well known that the accumulation of carbonaceous deposits on the catalyst is one of the main causes of the catalyst deactivation [11,21,26]. It has also been known that the Brønsted acid sites are

Table 2
Product distributions over the tested catalysts.

	Nano-CAT	Micro-CAT	Nano-CAT	Micro-CAT
Concentration of ethanol	95(v) %	95(v) %	45(v) %	45(v) %
Carrier-gas	35 ml/min	35 ml/min	0	0
WHSV (h^{-1})[a]	1.0	1.0	0.8	0.8
Time on stream (h)	420	100	260	50
Gas phase (mol%)				
Ethylene	98.67	98.02	97.57	95.98
Diethyl ether	0.04	0.05	0.50	2.04
Ethane	0.04	0.08	0.07	0.14
Acetaldehyde	Trace	Trace	Trace	Trace
Ethanol	0.56	1.08	0.46	0.53
C_3	0.23	0.15	0.54	0.52
C_4	0.27	0.26	0.50	0.59
C_5	0.05	0.06	0.07	0.19
$>C_6$	0.06	0.07	0.12	0.19
Methane	Trace	Trace	Trace	Trace
Liquid phase (mol%)				
Water	99.74	99.63	99.67	98.34
Ethanol	0.21	0.36	0.31	1.60
Acetaldehyde	0.05	Trace	Trace	Trace
Diethyl ether	Trace	Trace	Trace	0.05
Selectivity for ethylene (%)	98.69	98.71	96.48	93.00
Conversion of ethanol (%)	99.20	97.79	98.27	92.92

[a] WHSV was based on the component of ethanol; reaction temperature: 240 °C.

active sites for the dehydration of ethanol into ethylene [11], and ethylene is easy to polymerize on the strong Bronsted acid sites of HZSM-5 [23–25].

For the micro-CAT, most of the strong Brønsted acid sites distribute inside the zeolite channels [22], and the crystal size of micro-CAT is much bigger than that of nano-CAT, which means that the reactant in the micro-CAT needs to pass longer distance than that in the nano-CAT. In other words, the diffusion path of product over or inside the micro-CAT is much longer than that over or inside the nano-CAT, which leads to the carbonaceous deposits. Therefore, the micro-CAT deactivated rapidly. Le Van Mao et al. also reported that the stability could be improved by eliminating the strong acid sites in the zeolite [7].

For the nano-CAT, short channel-length and low ratio of strong acid sites inside the channels (or pore apertures) to total strong acid sites (deduced from Table 1) favor the diffusion of the product. Thus, the activity of the nano-CAT is passivated slowly. Fig. 9 is TG curves of the used catalysts. The amounts of

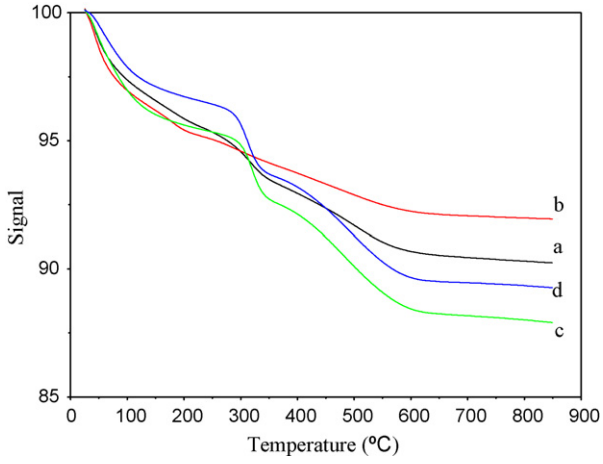

Fig. 9. TG curves of used catalysts: (a) nano-CAT under 95(v) % feedstock/630 h; (b) nano-CAT under 45(v) % feedstock/320 h; (c) micro-CAT under 95(v) % feedstock/144 h; (d) micro-CAT under 45(v) % feedstock/80 h.

carbonaceous deposits per hour on nano-CAT under 95(v) % feedstock/630 h, nano-CAT under 45(v) % feedstock/320 h, micro-CAT under 95(v) % feedstock/144 h, and micro-CAT under 45(v) % feedstock/80 h are 0.008%, 0.011%, 0.056%, and 0.095%, respectively. This further explains the reason for the high stability over nanoscale HZSM-5 catalyst.

4. Conclusion

Compared with the microscale HZSM-5 zeolite catalyst during the dehydration of bio-ethanol into ethylene at 240 °C under atmospheric pressure, the nanoscale HZSM-5 zeolite catalyst exhibited good coke-resistance and stability.

Acknowledgements

The project was financially supported by the program for New Century Excellent Talent in University (NECT-04-0268), the program for Key Lab of Universities of Liaoning Province and the 111 project.

References

[1] N.K. Kochar, R. Merims, A.S. Padia, Chem. Eng. Progr. 77 (1981) 66.
[2] R. Le Van Mao, and L.H. Dao, U.S. Patent 4,698,452 (1987).
[3] R. Le Van Mao, T.M. Nguyen, G.P. McLaughlin, Appl. Catal. 48 (1989) 265.
[4] R Le Van Mao, U.S. Patent 4,873,392 (1989).
[5] R.Le Van Mao, T.M. Nguyen, U.S. Patent 4,847,223 (1989).
[6] R. Le Van Mao, P. Levesque, G.P. McLaughlin, L.H. Dao, Appl. Catal. 34 (1987) 163.
[7] T.M. Nguyen, R. Le Van Mao, Appl. Catal. 58 (1990) 119.
[8] L.R. Pan, Chin. Petrochem. Technol. 16 (1987) 764.
[9] W.R. Moser, R.W. Thompson, C.C. Chiang, H. Tong, J. Catal. 117 (1989) 19.
[10] S. Bun, S. Nishiyama, S. Tsuruya, M. Masai, Appl. Catal. 59 (1990) 13.
[11] C.B. Phillips, R. Datta, Ind. Eng. Chem. Res. 36 (1997) 4466.
[12] D.S. Zhang, R.J. Wang, X.X. Yang, Catal. Lett. 124 (2008) 384.
[13] M. Yanmamura, K. Chaki, T. Wakatsuki, H. Okado, K. Fujimoto, Zeolites 14 (1994) 643.
[14] X.B. Zhao, X.W. Guo, X.S. Wang, Energy Fuels 20 (2006) 1388.
[15] P.Q. Zhang, X.S. Wang, X.W. Guo, H.C. Guo, L.P. Zhao, Y.K. Hu, Catal. Lett. 92 (2004) 63.
[16] L.P. Sun, X.W. Guo, M. Liu, X.S. Wang, Appl. Catal. A: Gen. 355 (2009) 184.
[17] X.Q. Wang, X.S.Wang, X.W. Guo, Chinese Patent CN 1,240,193 (2000).
[18] K. Wang, X.S. Wang, G. Li, Catal. Commun. 8 (2007) 324.
[19] T. Kawai, K.M. Jiang, T. Ishikawa, J. Catal. 159 (1996) 288.
[20] I. Takahara, M. Saito, M. Inaba, K. Murata, Catal. Lett. 105 (2005) 249.
[21] A.T. Aguayo, A.G. Gayubo, A. Atutxa, M. Olazar, J. Bilbao, Ind. Eng. Chem. Res. 41 (2002) 4216.
[22] T. Armaroli, L.J. Simon, Appl. Catal. A: Gen. 306 (2006) 78.
[23] H.G. Karge, M. Laniecki, M. Ziolek, G. Onyestyak, A. Kiss, P. Kleinschmit, M. Siray, in: A. Jacobs, R.A. van Santen (Eds.), Proceedings of the 8th International Conference on Zeolites, July 1989, vol. 30, Elsevier, Amsterdam, 1989, , pp. 1327–1338, Paper No. 130.
[24] M. Guisnet, P. Magnoux, Stud. Surf. Sci. Catal. 88 (1994) 53.
[25] J.G. Post, H.C. van Hooff, Zeolites 4 (1984) 9.
[26] S.A. Tabak, S. Yurchak, Catal. Today 6 (1990) 307.